

This is the peer reviewed version of the following article:

Nonempirical range-separated hybrid functionals for solids and molecules / Skone, Jonathan H.; Govoni, Marco; Galli, Giulia. - In: PHYSICAL REVIEW. B. - ISSN 2469-9950. - 93:23(2016), pp. 235106-235106. [10.1103/physrevb.93.235106]

Terms of use:

The terms and conditions for the reuse of this version of the manuscript are specified in the publishing policy. For all terms of use and more information see the publisher's website.

03/05/2024 12:54

(Article begins on next page)



CHORUS

This is the accepted manuscript made available via CHORUS. The article has been published as:

Nonempirical range-separated hybrid functionals for solids and molecules

Jonathan H. Skone, Marco Govoni, and Giulia Galli
Phys. Rev. B **93**, 235106 — Published 3 June 2016

DOI: [10.1103/PhysRevB.93.235106](https://doi.org/10.1103/PhysRevB.93.235106)

Nonempirical Range-separated Hybrid Functionals for Solids and Molecules

Jonathan H Skone,^{1,2} Marco Govoni,^{1,2} and Giulia Galli^{1,2,*}

¹*Institute for Molecular Engineering, University of Chicago, 5801 South Ellis Avenue, Chicago, IL 60637*

²*Materials Science Division, Argonne National Laboratory, Argonne, IL 60439*

(Dated: May 6, 2016)

Dielectric-dependent hybrid (DDH) functionals were recently shown to yield accurate energy gaps and dielectric constants for a wide variety of solids, at a computational cost considerably less than that of GW calculations. The fraction of exact exchange included in the definition of DDH functionals depends (self-consistently) on the dielectric constant of the material. Here we introduce a range-separated (RS) version of DDH functionals where short and long-range components are matched using system dependent, non-empirical parameters. We show that RS DDHs yield accurate electronic properties of inorganic and organic solids, including energy gaps and absolute ionization potentials. Furthermore we show that these functionals may be generalized to finite systems.

I. INTRODUCTION

To hasten the discovery of new materials with optimal properties for applications such as optical and electronic devices, catalysis, quantum information, and photovoltaics, the reliance on theory to support and direct experimental efforts is essential. The determination of the ground and excited state electronic properties relevant to such applications, require a high level of accuracy, ideally at a modest computational cost. Density functional theory (DFT)¹ has long been one of the main methodologies of choice as it provides a reasonable compromise between accuracy and computational efficiency. Some of the most accurate functionals include an admixture of local and nonlocal exchange and are referred to as hybrid functionals.² The latter have been widely used for molecules and less so to model extended systems. The slower adoption of hybrid functionals for condensed phases is a consequence of using plane-wave basis sets in most condensed matter calculations, and of the lack of nonempirical parameters for constructing accurate hybrid functionals.³ Indeed the treatment of the non-local exchange operator within periodic boundary conditions by using a plane-wave basis set is computationally demanding. In the last decade, however, due in part to several methodological advances,^{4–7} hybrid functionals have been increasingly used to investigate a variety of periodic systems within a plane-wave pseudopotential framework.

Addressing the need for improved accuracy of DFT for condensed systems, a new class of functionals was recently proposed, with parameters defined using the dielectric constant of the system.^{8–13} This class of functionals, referred to as dielectric-dependent hybrid (DDH) functionals, can yield accurate electronic structures of solids, at considerably less cost with respect, e.g. to GW based methods. Among DDHs, are those where the dielectric constant is determined self-consistently,^{8,9,12} which are referred to as sc-hybrid.¹² This sc-hybrid functional has found recent use in the study of pristine oxides,^{12,14,15} defects in oxides,^{16,17} nitrides,^{18,19} aqueous solutions,²⁰ and spin-defects in wide band gap semiconductors.²¹ The adaptation of non self-consistent

DDHs to a time-dependent framework was recently pursued by Yang *et al.*,²² Ferrari *et al.*,²³ and Refaely-Abramson *et al.*,²⁴ with the goal of obtaining optical spectra of solids. Another recent study by Shimazaki *et al.*²⁵ explored the possibility of defining a *local* DDH functional where the fraction of exact-exchange is site dependent. Though their initial prescription using atom-centered basis functions is perhaps oversimplified, the proposal of Ref 25 is an interesting step towards describing *heterogenous systems* with DDH functionals.

In this paper we introduce a range-separated (RS) version of DDH functionals where short and long-range components are matched using system dependent, nonempirical parameters. We assess the accuracy of RS-DDH functionals for the electronic properties of inorganic materials and molecular crystals, and we present calculations for energy gaps and absolute ionization potentials. We show that range-separated DDH functionals are superior to full-range DDH functionals for the energy gaps of inorganic solids, while both full and range separated hybrids yield equally accurate results for the gaps and ionization potentials of molecular crystals. In addition, we show that RS-DDH can be generalized to finite systems.

The rest of the paper is organized as follows. Section II describes the range-separated DDH functional along with the computational details used in this work. Section III presents results obtained using nonempirical parameters for the range-separated and full-range DDH functionals for a set of inorganic solids, molecular crystals, and finite systems. Section IV summarizes our results, and provides our conclusions.

II. METHOD

A. Range-separated dielectric-dependent hybrid functionals

We use a Generalized Kohn Sham (GKS) framework where we determine an effective screening of the Coulomb potential by computing the dielectric response of the system.

The GKS nonlocal potential $v_{\text{GKS}}(\mathbf{r}, \mathbf{r}')$ entering the Kohn-Sham (KS) Hamiltonian is given by:

$$v_{\text{GKS}}(\mathbf{r}, \mathbf{r}') = v_H(\mathbf{r}) + v_x(\mathbf{r}, \mathbf{r}') + v_c(\mathbf{r}) + v_{\text{ext}}(\mathbf{r}) \quad (1)$$

where $v_H(\mathbf{r})$ is the Hartree, $v_x(\mathbf{r}, \mathbf{r}')$ is the nonlocal exchange potential, $v_c(\mathbf{r})$ is the correlation potential, and $v_{\text{ext}}(\mathbf{r})$ is the attractive Coulomb potential to the nuclei.

The nonlocal exchange potential $v_x(\mathbf{r}, \mathbf{r}')$ is partitioned into long-range (lr) and short-range (sr) components where α and β , define the fraction of exact exchange admixed to semilocal exchange in the lr and sr components, respectively:

$$v_x(\mathbf{r}, \mathbf{r}') = \alpha v_x^{\text{lr-ex}}(\mathbf{r}, \mathbf{r}'; \mu) + \beta v_x^{\text{sr-ex}}(\mathbf{r}, \mathbf{r}'; \mu) + (1 - \alpha)v_x^{\text{lr}}(\mathbf{r}; \mu) + (1 - \beta)v_x^{\text{sr}}(\mathbf{r}; \mu). \quad (2)$$

The screening parameter μ defines how the lr and sr components are bridged. We use the error function to define the range separation of the Coulomb interaction, namely:

$$v_x^{\text{lr-ex}}(\mathbf{r}, \mathbf{r}'; \mu) = -\rho(\mathbf{r}, \mathbf{r}') \frac{\text{erf}(\mu|\mathbf{r} - \mathbf{r}'|)}{|\mathbf{r} - \mathbf{r}'|} \quad (3)$$

and

$$v_x^{\text{sr-ex}}(\mathbf{r}, \mathbf{r}'; \mu) = -\rho(\mathbf{r}, \mathbf{r}') \frac{\text{erfc}(\mu|\mathbf{r} - \mathbf{r}'|)}{|\mathbf{r} - \mathbf{r}'|}, \quad (4)$$

where $\rho(\mathbf{r}, \mathbf{r}')$ is the density matrix. The semilocal exchange potentials, $v_x^{\text{sr}}(\mathbf{r}; \mu)$ and $v_x^{\text{lr}}(\mathbf{r}; \mu)$, depend only on the density $\rho(\mathbf{r})$ and its gradient. Here we adopt the PBE²⁶ approximation of the semilocal exchange $v_x(\mathbf{r})$ and correlation $v_c(\mathbf{r})$. Many of the commonly used exchange functional forms may be recovered from Eq. 2. For example, when $\alpha = \beta = \mu = 0$, one obtains the PBE semilocal functional. If $\alpha = 1$, $\beta = 0$, and $\mu \rightarrow \infty$ one obtains the KS equations with the exact-exchange potential (EXXc²⁷). If instead $\alpha = 0.25$, $\beta = 0$, and $\mu \rightarrow \infty$ the PBE0 hybrid functional is recovered. Short-range hybrid functionals ($\alpha = 0$) may also be easily obtained e.g. HSE06²⁸ where $\beta = 0.25$ and $\mu = 0.11 \text{ bohr}^{-1}$ or sX-LDA²⁹ where $\beta = 1$, $\alpha = 0$, and the Thomas-Fermi screening function is used instead of the error function³⁰. Examples of long-range hybrid functionals ($\alpha \neq 0$) include the empirical CAM-B3LYP functional,³¹ where $\alpha = 0.46$, $\beta = 0.19$, $\mu = 0.33 \text{ bohr}^{-1}$, as well as LC- μ PBE,³² where $\alpha = 1$, $\beta = 0$, and $\mu = 0.4 \text{ bohr}^{-1}$. The screened-exchange methodology of Robinson *et al.*³³ and subsequent works,^{29,34,35} present a similar approach to the description of electronic screening, but the function used to partition the Coulomb operator and the asymptotic long-range limit of the Coulomb potential differ from those used here.

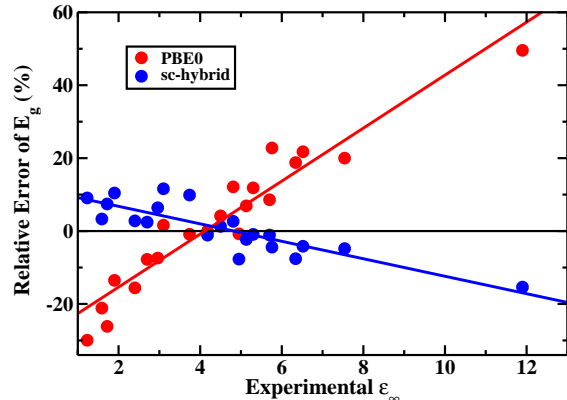


FIG. 1: (Color online) Plot of the signed relative error in the electronic gap (E_g) for a set of semiconductors and insulators (see Table II) computed at the PBE0 (red circles and line) and sc-hybrid (blue circles and line) levels of theory as a function of the experimental electronic dielectric constant ϵ_∞ . The CoO material was removed from this analysis since the sc-hybrid functional appears to be ill-suited for systems with localized d-electrons at the valence band edge.

The goal of the present work is to generalize the self-consistent dielectric-dependent hybrid functional (sc-hybrid)¹² to a range-separated form. To do so we first compare results obtained with the PBE0 global hybrid ($\alpha = 0.25$) and the sc-hybrid, where the global fraction of exchange is inversely proportional to the self-consistently determined electronic dielectric constant (ϵ_∞), namely

$$\alpha = \frac{1}{\epsilon_\infty}. \quad (5)$$

As discussed in Ref. 12, Eq. (5) can be obtained from the static COHSEX self-energy,³⁶ by approximating the screened Coulomb interaction W with an effective screened interaction, where the inverse microscopic dielectric function is replaced by the inverse macroscopic dielectric constant:

$$W(\mathbf{r}, \mathbf{r}') = \int d\mathbf{r}'' \epsilon^{-1}(\mathbf{r}, \mathbf{r}'') v(\mathbf{r}'', \mathbf{r}') \approx \frac{\alpha}{|\mathbf{r} - \mathbf{r}'|}. \quad (6)$$

We previously found that for a set of diverse semiconductors and insulators the mean absolute relative error (MARE) in the computed energy gaps was $\sim 17\%$ and $\sim 7.0\%$ when using PBE0 and the sc-hybrid, respectively. Fig. 1 shows the signed relative error of the predicted electronic gaps with respect to experiment, as a function of the experimental dielectric constant. For $\epsilon_\infty > 4$ the PBE0 (sc-hybrid) over- (under-) estimates the experimental energy gap, and vice versa for $\epsilon_\infty < 4$. Hence for systems with $\epsilon_\infty^{-1} = \alpha < (>) 0.25$, increasing

(lowering) α from 0.25 may improve the agreement with experimental photoemission gaps.

Based on this observation, we defined a new class of DDH functionals having the general form of Eq. (2), where we set the long range fraction $\alpha = \epsilon_\infty^{-1}$ and the short range fraction $\beta = 0.25$ (as in PBE0). Within this framework, the approximate $W(\mathbf{r}, \mathbf{r}')$ becomes:

$$W(\mathbf{r}, \mathbf{r}') \approx \frac{\epsilon_\infty^{-1}}{|\mathbf{r} - \mathbf{r}'|} + (\beta - \epsilon_\infty^{-1}) \frac{\text{erfc}(\mu|\mathbf{r} - \mathbf{r}'|)}{|\mathbf{r} - \mathbf{r}'|}, \quad (7)$$

where the first term on the right hand side of Eq. (7) is the same as the sc-hybrid functional of Ref. 12 and the second term is a short-range correction to the Coulomb potential. The numerator of Eq. (7) is plotted as a function of μ in Fig. S1 of the Supplemental Material. Note that the expression of Eq. (7) is general, and β is in principle a parameter to be determined; here we chose $\beta = 0.25$ based on the results of Fig. 1. The plot indicates that a value of μ in the range $(0, +\infty)$ exists which may improve the description of the electronic gaps with respect to both PBE0 and sc-hybrid functionals. We note that the long-range limit of the RS DDH functional defined here is physically correct; however the short-range limit of the exchange is not correctly unscreened, but rather attenuated by the PBE0 fraction of exchange (0.25). This attenuation factor of the exchange amounts, in practice, to introducing an approximate form of short-range correlation in the functional.

We explored three different non-empirical choices of μ which do not require any optimization procedure, nor calculations for charged systems, unlike e.g. other definitions of range-separated hybrid functionals,^{37–39} or Koopman complaint functionals.^{40–42}

(I.) Assuming that a homogeneous spatial distribution of the valence electrons is a good approximation of the valence charge density of the system, we defined a screening length related to the average volume occupied by a valence electron:

$$\mu_{WS} = \frac{1}{r_s} = \left(\frac{4\pi n_v}{3} \right)^{\frac{1}{3}} \quad (8)$$

where n_v is the valence electron density, and r_s is the Wigner-Seitz radius.

(II.) Alternatively, we used the Thomas-Fermi screening parameter (μ_{TF}):

$$\mu_{TF} = \frac{1}{2} k_{TF} = \left(\frac{3n_v}{\pi} \right)^{\frac{1}{6}} \quad (9)$$

where $k_{TF} = 2 \left(\frac{3n_v}{\pi} \right)^{\frac{1}{6}}$ is the Thomas-Fermi screening length. Note that in the definition of both μ_{WS} and μ_{TF} , atomic units are used,⁴³ and $\mu_{TF} = 0.781593 \sqrt{\mu_{WS}}$.

(III.) Finally we defined a range separation parameter μ obtained from the long-range decay of the diagonal elements of the dielectric matrix, as computed from first principles using the linear response techniques proposed

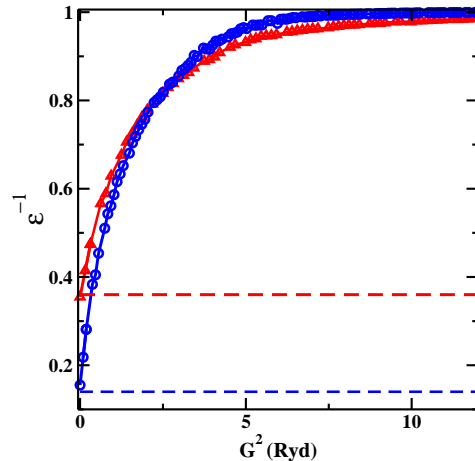


FIG. 2: (Color online) Plot of the inverse diagonal dielectric function (ϵ^{-1}) in Fourier space as a function of G^2 for a prototypical insulator MgO (red triangles and line) and a prototypical small gap semiconductor AIP (blue circles and line). The dashed lines correspond to ϵ_∞^{-1} screening that is seen over all inter-electronic distances for the global sc-hybrid.

in Ref. 44 and implemented in the WEST code.⁴⁵ Fig. 2 shows the dielectric function ($\epsilon^{-1}(\mathbf{G}, \mathbf{G}')$) computed neglecting the non-diagonal components for a prototypical semiconductor AIP, and a prototypical insulator MgO. We used two model functions to fit $\epsilon^{-1}(\mathbf{G}, \mathbf{G}')$ and extract screening parameters that we collectively refer to as μ_{PDEP} ⁴⁶: the Thomas-Fermi screening model (corresponding to a Yukawa potential) and the complementary error function. Using the former, the screened Coulomb interaction is:

$$W(\mathbf{r}, \mathbf{r}') \approx \frac{\epsilon_\infty^{-1}}{|\mathbf{r} - \mathbf{r}'|} + (1 - \epsilon_\infty^{-1}) \frac{e^{-k_{TF}|\mathbf{r} - \mathbf{r}'|}}{|\mathbf{r} - \mathbf{r}'|} \quad (10)$$

The fit of the dielectric function was carried out in Fourier space:

$$\epsilon_{TF}^{-1}(\mathbf{G}) = \epsilon_\infty^{-1} + (1 - \epsilon_\infty^{-1}) \frac{G^2}{G^2 + k_{TF}^2}. \quad (11)$$

If instead of the TF screening model, the complementary error function is used to fit $\epsilon^{-1}(\mathbf{G}, \mathbf{G}')$, we obtain:

$$\epsilon_{erfc}^{-1}(\mathbf{G}) = \epsilon_\infty^{-1} + (1 - \epsilon_\infty^{-1}) (1 - e^{-\frac{G^2}{4\mu^2}}). \quad (12)$$

The performance of the RS DDH functional obtained by substituting in Eq. (2) $\alpha = \epsilon_\infty^{-1}$, $\beta = 0.25$ and for each of the three μ parameters described above (namely μ_{WS} , μ_{TF} and μ_{PDEP}) will be discussed in Section III A for inorganic semiconductors and insulators; and in Section III B for molecular crystals. We will show that

our results are largely insensitive to the three choices of μ , which turn out to be similar to each other for all systems examined here.

B. Computational details

The evaluation of the electronic dielectric constant was carried out within an all-electron approach using the coupled perturbed Kohn-Sham (CPKS)^{47,48} equations (the coupled-perturbed Hartree-Fock method (CPHF)^{49–51} extended to DFT) as implemented in the CRYSTAL14⁵² electronic structure package, where we explicitly computed ϵ beyond the random phase approximation (RPA) by evaluating $f_{xc} = \frac{\delta v_{xc}}{\delta \rho}$, i.e. the functional derivative of the nonlocal potential v_{xc} . The effect of including f_{xc} in the evaluation of ϵ was discussed in Ref. 12. The dielectric constant determined self-consistently was then used in the range-separated functional of Eq. (7) as implemented in both the CRYSTAL14 and in the Quantum-ESPRESSO package.⁵³ We note that a denser k -point mesh is required for the convergence of the electronic dielectric constants than for the KS eigenvalues (see Supplemental Material for details).

The WEST⁴⁵ code was used to compute the dielectric matrix using 1024 eigenpotentials for each system considered here, unless otherwise noted. These calculations were carried out at the Γ -point for a supercell of appropriate size.

For the all-electron calculations, we used Gaussian basis sets, modified starting from Alhrich's def2-TZVPP molecular basis,⁵⁴ with the only exception of rare gases Ne and Ar basis sets, which were modified starting from the def2-QZVPD set.⁵⁵ For Co and Ni we used the def2-TZVP modified basis sets of Bredow *et al.*⁵⁶ For the plane-wave calculations, we adopted norm-conserving pseudopotentials of the Troullier-Martins type,⁵⁷ where for the transition metal atoms, unless otherwise noted, the $(n-1)s$ and $(n-1)p$ electrons were included in the valence (n is the highest principal quantum number). Plane-wave kinetic energy cutoffs and localized Gaussian basis sets employed here can be found in the Supplemental Material. All calculations were performed at the experimental geometry and $T = 0\text{K}$, without consideration of zero-point vibrational effects. In the case of transition metals we excluded any semi-core $(n-1)s$ and $(n-1)p$ electrons from the definition of the valence electron density that is used to determine μ_{WS} and μ_{TF} .

To obtain the ionization potential of molecular crystals, both all-electron bulk calculations with no surface present were used, as well as slab model calculations. The latter, carried out using a plane-wave pseudopotential basis set, were necessary to set an absolute scale with respect to vacuum, through electrostatic potential alignments. The supercell size in the direction perpendicular to the interface was chosen so as to ensure a converged value of the electrostatic potential (see the Supplemental Material for details).

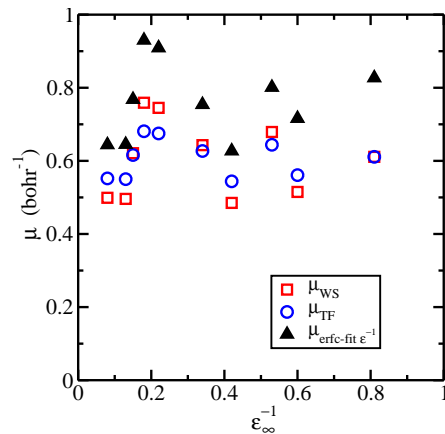


FIG. 3: (Color online) Screening parameters μ (as defined in the text) are plotted versus the inverse electronic dielectric constant for a set of inorganic semiconductors and insulators. The Wigner-Seitz screening parameter μ_{WS} (red open squares) Eq. (8), the Thomas-Fermi screening parameter μ_{TF} (blue open circles) Eq. (9), and $\mu_{\text{erc-fit } \epsilon^{-1}}$ (black filled triangles) obtained from a fit to Eq. (12), are shown.

In our calculation of gas phase ionization potentials discussed in Section III C, a plane-wave basis was used along with a Makov-Payne⁵⁸ correction to properly align the orbital eigenvalues with the vacuum level position. Molecular polarizabilities were evaluated at the PBE level of theory. Although the values of the polarizability varies with respect to the level of theory applied, the inverse cube root used to define the inverse molecular polarizability radius exhibits a negligible variation with respect to the level of theory. The screening parameters determined from the optimally tuned range-separated hybrid (OT-RSH) procedure described in Ref. 38 were evaluated in a planewave basis with a Makov-Payne correction applied, using the Quantum-ESPRESSO package.

III. RESULTS AND DISCUSSION

A. Inorganic semiconductors and insulators

The non empirical values of the screening parameters for a diverse set of inorganic semiconductors and insulators as obtained from Eq. (8) and Eq. (9) are provided in Table I. For a subset of systems the screening parameters were also computed by fitting the long-range decay of the dielectric function to either Eq. 11 or to Eq. 12, and these are listed under the column heading μ_{PDEP} . The parameters μ_{PDEP} are in general larger than μ_{WS} and μ_{TF} , which are similar to each other. However as we will see below, functionals defined with each of these three choices yield very similar results for the electronic gaps. A graphical comparison of screening parameters as a function of the dielectric constant is given in Fig. 3.

TABLE I: The dielectric constant (ϵ_∞) determined self-consistently as described in Ref. 12 for the set of semiconductors and insulators listed in the first column, is given in column 2. The screening parameters (μ) used in the RSH functional form of Eq. (7) are listed in units of bohr⁻¹ in columns 3-6. (See text)

	ϵ_∞	μ_{WS}	μ_{TF}	μ_{PDEP}	
				$\mu_{\text{erfc-fit}}$	$\mu_{\text{TF-fit}}$
Si	11.76	0.50	0.55	0.64	0.64
AlP	7.23	0.50	0.55	0.65	0.64
SiC	6.50	0.62	0.62	0.77	0.77
TiO ₂	6.56	0.68	0.65		
NiO	5.49	0.82	0.71		
C	5.61	0.76	0.68	0.93	0.97
CoO	4.92	0.78	0.69		
GaN	5.14	0.60	0.61		
ZnS	4.95	0.65	0.63		
MnO	4.45	0.72	0.66		
WO ₃	4.72	0.66	0.63		
BN	4.40	0.75	0.68	0.91	0.95
HfO ₂	3.97	0.66	0.63		
AlN	4.16	0.49	0.55		
ZnO	3.46	0.78	0.69		
Al ₂ O ₃	3.01	0.71	0.66		
MgO	2.81	0.64	0.63	0.75	0.72
LiCl	2.77	0.53	0.57		
NaCl	2.29	0.49	0.54	0.63	0.64
LiF	1.86	0.68	0.64	0.80	0.83
H ₂ O	1.68	0.55	0.58	0.52	0.53
Ar	1.66	0.52	0.56	0.72	0.73
Ne	1.21	0.61	0.61	0.83	0.89

Photoemission gaps of inorganic semiconductors and insulators⁵⁹ computed with the μ parameters of Table I are reported in Table II. For most systems, irrespective of the choice of the system dependent screening parameter μ , the RSH functional yields improved electronic gaps over the already accurate full-range sc-hybrid functional. The only exceptions, are some transition metal oxides where partially occupied d-orbitals dominate the character of the valence band—most notably CoO as well as FeO (not shown) and to a lesser extent NiO and MnO⁶⁰. If these systems are not included in the assessment of the RSH functional quality, a more noticeable improvement is obtained, as shown in Table S3, and by comparison with self-consistent GW results from Shishkin *et al.*⁶¹ (see column 7 of Table II). As shown in Table S3, for this subset of solids the MARE for all definitions of μ are lower than that of the sc-GW results.

In the case of μ_{PDEP} , we only tabulate the computed electronic gaps for the complementary error function fit, using Eq. (12), labeled as $\mu_{\text{erfc-fit}}$ in Table II since those

obtained from fitting to the Thomas-Fermi screening model (Eq. (12)) are nearly identical. Overall the RSH results using $\mu_{\text{erfc-fit}}$ appear to be very similar to those of the sc-hybrid functional.

The small differences between the MAEs of results obtained with the various choices of μ warrant further analysis to determine whether these apparent differences are statistically meaningful. We determined the confidence interval over which one methodology MAE is statistically different from another one by performing a Wilcoxon signed-rank test⁸⁵ between pairs of methods; a p-value below 0.05⁸⁶ was chosen to indicate that indeed the two sets of results exhibit different MAEs (i.e. differences are not due to chance). We found that the p-values computed between the MAE obtained with different choices of μ are all larger than 0.05, indicating that the three choices of μ yield the same result. For any of the RS-DDH functionals compared to the global sc-hybrid or PBE0 functional, all p-values are below 0.05 indicating that the improvement in the MAE of RSH functionals relative to sc-hybrid or PBE0 is statistically significant. For a summary of all p-values between pairs of methods for the full set of 23 systems listed in Table II and for a subset of these solids where transition metal oxides are removed, see Table S4 and Table S5, respectively, in the Supplemental Material.

To assess how the electronic gap depends on the sr fraction of exchange we examined the gap dependence for two systems with $\epsilon > 4$ and $\epsilon < 4$, respectively. In Fig. 4 we set $\alpha = \epsilon_\infty^{-1}$ in the RSH functional form and we show the behavior of the signed electronic gap error as a function of μ and β . The prototypical semiconductor (AlP) and insulator (MgO) show opposite behaviors and the curvature of the minimum error (white region) is concave for the former and convex for the latter. As $\mu \rightarrow \infty$ the sc-hybrid functional is recovered and an overestimation (underestimation) of the gap for insulating MgO (semiconducting AlP) is obtained.

B. Molecular Crystals

The dielectric constants determined self-consistently for a set of molecular crystals are shown in Table III along with the screening parameter μ_{TF} , which is found to be nearly constant at 0.58 bohr⁻¹ and $\mu_{\text{erfc-fit}}$, which is similar albeit slightly smaller than μ_{TF} . The screening parameters μ are shown as a function of ϵ_∞^{-1} in Fig. 5. Comparison between different levels of theory for the computed dielectric constants are shown in Table S2 of the Supplemental Material. In general, the PBE results yield the poorest agreement with experiment, with PBE0 showing a marked improvement, and the DDH functionals performing the best.

For a subset of optically anisotropic molecular crystals, we compare in Table IV the dielectric tensor components computed at different levels of theory with that obtained experimentally. As expected, the values of the tensor components vary depending on the level of

TABLE II: The Kohn-Sham (KS) energy gaps (eV) evaluated with hybrid functionals are compared with the experimental (Exp.) electronic gaps for a wide range of semiconductors and insulators. The experimental values correspond to either photoemission measurements or to optical measurements where the excitonic contributions were removed, with alumina being the only exception. The KS gaps were computed as the single particle energy difference of the conduction band minimum and the valence band maximum. The sc-hybrid heading refers to hybrid calculations where the fraction of exact-exchange is the self-consistent ϵ_∞ . The RSH columns correspond to the electronic gap evaluated with the range separation scheme described in Section II, and the screening parameters μ_{WS} (Eq. 8), μ_{TF} (Eq. 9), and $\mu_{erfc-fit}$ (Eq. 12). The self-consistent quasiparticle (scGW) gaps are taken from Ref. 61.

ME, MAE, MRE, and MARE are the mean, mean absolute, mean relative, and mean absolute relative error, respectively. The experimental geometry was used in all calculations. Note that CoO, NiO, and MnO are magnetic with AFM-II magnetic ordering. The structure/polytype used for each system is the same as in Table I of Ref. 12.

	PBE0	sc-hybrid	RSH	RSH	RSH	scGW ⁶¹	Exp.
			μ_{WS}	μ_{TF}	$\mu_{erfc-fit}$		
Si	1.75	0.99	1.03	1.02	1.01	1.24	1.17 ⁶²
AlP	2.98	2.37	2.43	2.42	2.40	2.57	2.51 ⁶³
SiC	2.91	2.29	2.32	2.32	2.31	2.53	2.39 ⁶⁴
TiO ₂	3.92	3.05	3.16	3.17			3.3 ⁶⁵
NiO	5.28	4.11	4.45	4.51			4.3 ⁶⁶
C	5.95	5.42	5.44	5.45	5.43	5.79	5.48 ^{67 a}
CoO	4.53	3.62	3.92	3.98			2.5 ⁷¹
GaN	3.68	3.26	3.30	3.30		3.27	3.29 ⁷²
ZnS	4.18	3.82	3.85	3.86		3.60	3.91 ⁶²
MnO	3.87	3.60	3.65	3.49			3.9 ⁷³
WO ₃	3.76	3.47	3.49	3.49			3.38 ⁷³
BN	6.51	6.33	6.33	6.34	6.33	6.59	6.4 ⁷⁴
HfO ₂	6.65	6.68	6.67	6.67			5.84 ⁷⁵
AlN	6.31	6.23	6.22	6.23			6.28 ⁷⁶
ZnO	3.41	3.78	3.75	3.67		3.2	3.44 ⁷⁷
Al ₂ O ₃	8.84	9.71	9.63	9.61			8.8 ⁷⁸
MgO	7.25	8.33	8.23	8.22	8.27	8.12	7.83 ⁷⁹
LiCl	8.66	9.62	9.52	9.54			9.4 ⁸⁰
NaCl	7.26	8.84	8.60	8.66	8.71		8.6 ⁸¹
LiF	12.18	15.69	15.24	15.18	15.42	14.5	14.2 ⁸²
H ₂ O	7.92	11.49	10.89	10.94	10.84		10.9 ⁸³
Ar	11.20	14.67	14.12	14.20	14.41	13.9	14.2 ⁸⁴
Ne	15.20	23.67	21.44	21.44	22.28	21.4	21.7 ⁸⁴
ME (eV)	-0.40	0.32	0.18	0.19			–
MAE (eV)	1.08	0.42	0.29	0.30			–
MRE (%)	6.2	3.7	3.4	3.5			–
MARE (%)	17.1	7.5	6.4	6.5			–

^a The exp. QP gap reported here does not account for the ZPE gap renormalization, which has been shown to be nonnegligible for diamond.^{68–70}

theory, but they all exhibit similar errors with respect to experiment. At variance with inorganic materials,¹² the dielectric constant of organic crystals shows a weaker dependence on the functional used. A notable exception is the charge-transfer molecular crystal DBTTF-TCNQ, where along the charge transfer direction, $\epsilon_{xx}(\infty)$ varies from 42.38 (PBE) to 11.08 (PBE0). Clearly for charge-transfer molecular crystals the use of a self-consistently determined dielectric screening and the corresponding

set of wavefunctions are required to obtain accurate dielectric constants.⁹³

Below we discuss results obtained for electronic gaps, and vertical ionization potentials obtained using the parameters reported in Table III.

The computed electronic gaps are compared with experiment in Table V. In general all the DDH functionals give similar results; the reason why there is almost no

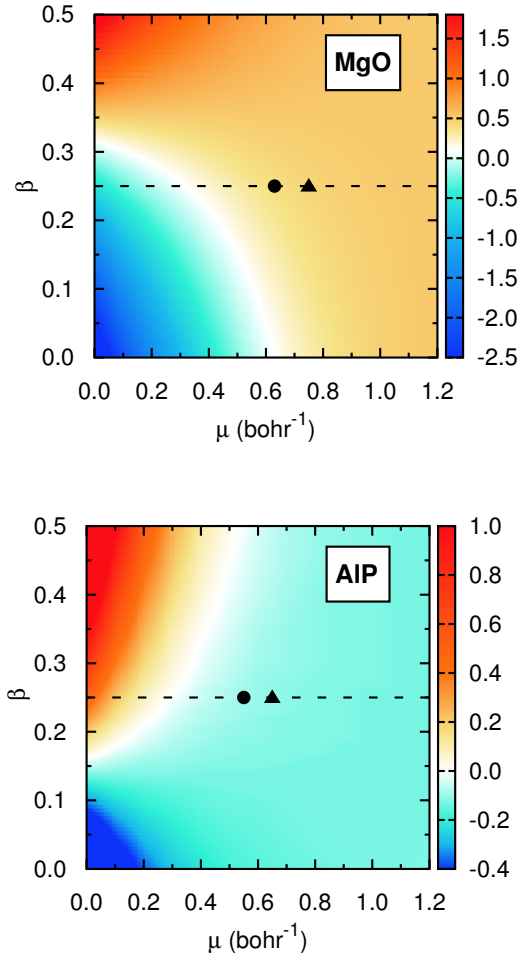


FIG. 4: (Color online) Signed electronic gap errors (theory - experiment), in units of eV, for a RSH functional defined by Eq. (7), as a function of two parameters: μ and β (see text). Results are reported for a prototypical insulator (MgO) with $\epsilon_\infty < 4$ and a semiconductor (AIP) with $\epsilon_\infty > 4$. Positive (negative) errors are indicated by shades of red (blue). The white shaded area corresponds to zero error with respect to experiment. The dashed black line corresponds to the fixed parameter space explored in the RS-DDH form where $\beta = 0.25$. The black circle and triangle indicate where the values of μ_{TF} and $\mu_{\text{erfc-fit}}$ fall, respectively.

variability between the full-range and range-separated hybrids for the organic molecular crystals stems from their inverse dielectric constant (0.2-0.35) which is close to the fraction of exchange adopted for the short-range limit (0.25), making the lr and sr limits of RSH very similar. To investigate the statistical significance of our results, we performed a paired test between the MAEs of the DDH functionals, showing that the MAEs of the full-range and the range-separated DDH functionals are not statistically significant (see Table S6 of Supplemental

TABLE III: The dielectric constant (ϵ_∞) determined self-consistently as described in Ref. 12 for the set of molecular crystals listed in the first column, is given in column 2. The screening parameters (μ) used in the RSH functional form of Eq. (7) are listed in units of bohr⁻¹ in columns 3-4. All μ have units of bohr⁻¹.

	Crystalline		
	ϵ_∞	μ_{TF}	$\mu_{\text{erfc-fit}}$
C ₁₄ H ₈ S ₄ -C ₁₂ H ₄ N ₄ (DBTTF-TCNQ)	11.07	0.58	
C ₆₀ (buckminsterfullerene)	4.29	0.61	0.57
C ₃₂ H ₁₈ N ₈ (phthalocyanine)	3.97	0.60	
C ₂₄ H ₈ O ₆ (α PTCDA)	3.45	0.61	
C ₂₂ H ₁₄ (pentacene)	3.36	0.59	
C ₂₀ H ₁₂ O ₂ (β quinacridone)	3.15	0.60	
C ₁₈ H ₁₂ (tetracene)	3.15	0.59	
C ₁₄ H ₁₀ (anthracene)	3.02	0.58	
C ₄₂ H ₂₈ (rubrene)	2.88	0.58	0.50
C ₁₀ H ₈ (naphthalene)	2.70	0.58	
C ₆ H ₆ (benzene)	2.40	0.57	0.54
NH ₃ (ammonia)	2.00	0.57	0.53
C ₂ H ₄ O ₂ (acetic acid)	1.88	0.60	
H ₂ O (ice)	1.68	0.58	0.52

Material), unlike the case of inorganic materials.

In a previous study,⁹⁴ it was observed that a fraction of exchange in the range of 0.31-0.35 yielded electronic gaps of organic semiconducting molecular crystals, such as pentacene, in very good agreement with experiment and GW calculations. Indeed, as mentioned above and shown in Table S2, the computed inverse dielectric constants of many of the semiconducting molecular crystals are centered around ~ 0.3 . We also note that the good performance of the PBE0-1/3 functional⁹⁵ for molecular crystals reported in the literature most likely stems from the 1/3 fraction of exact-exchange used being similar in value to the inverse dielectric constant of the molecular crystals.

Similar to what was done for two exemplary inorganic systems, we varied the sr fraction of Hartree-Fock exchange (β) together with the screening parameter (μ) for a molecular crystal (ice), to assess how the electronic gap depends on the coupling of these two quantities. Fig. 6 shows the 2D heat map of the signed electronic gap error for ice as a function of β and μ . A concave curvature of the minimum error (white region) similar to that of the inorganic insulator MgO with $\epsilon_\infty < 4$ was observed for ice.

We also evaluated the vertical ionization potential (vIP) of a subset of molecular crystals, namely rubrene, ice, and benzene, which are tabulated in Table VI. Slab calculations were used (see Method Section) in order to place the valence band obtained from plane-wave pseudopotential calculations on an absolute energy scale (see Table S7 of the Supplemental Material for the electro-

TABLE IV: The xx , yy , and zz components of the dielectric tensor (ϵ_∞) of the systems listed on the first row, computed at the PBE, PBE0, and sc-hybrid levels of theory and the corresponding experimental results.

	Anthracene			PTCDA			DBTTF-TCNQ		
	ϵ_{xx}	ϵ_{yy}	ϵ_{zz}	ϵ_{xx}	ϵ_{yy}	ϵ_{zz}	ϵ_{xx}	ϵ_{yy}	ϵ_{zz}
PBE	2.28	2.93	4.30	2.25	4.40	4.50	42.38	3.67	2.90
PBE0	2.22	2.83	4.10	2.12	4.10	4.12	11.08	5.82	2.72
sc-hybrid	2.21	2.80	4.02	2.11	4.06	4.08	26.28	3.54	2.81
Exp. ^{87,88}	2.42 ± 0.05	2.90 ± 0.05	4.07 ± 0.05	2.40	5.29	5.02			
Exp. ^{89,90}	2.62 ± 0.03	2.94 ± 0.03	4.08 ± 0.03	1.90		4.49			
Exp. ^{91,92}	2.51	2.99	4.11	2.28		3.73			

TABLE V: The Kohn-Sham (KS) energy gaps (eV) evaluated with the dielectric-dependent hybrid functionals, PBE and PBE0 are compared with the experimental electronic gaps for several molecular crystals. The experimental values are from photoemission measurements.

	PBE	PBE0	Hybrid	Hybrid	sc-hybrid	RSH	Exp.
	$\alpha = 0$	$\alpha = 0.25$	$\alpha = 1/\epsilon_\infty^{\text{PBE}}$	$\alpha = 1/\epsilon_\infty^{\text{PBE0}}$	$\alpha = 1/\epsilon_\infty^{\text{sc}}$	μ_{TF}	
DBTTF-TCNQ	0.16	0.74	0.26	0.45	0.31	0.33	
C60	1.27	2.34	2.11	2.27	2.26	2.26	2.3 ± 0.1 ⁹⁶
phthalocyanine (H ₂ Pc)	1.22	1.85	1.84	1.85	1.85	1.85	2.2 ± 0.2 ⁹⁷
PTCDA	1.41	2.53	2.62	2.72	2.73	2.73	2.74 ± 0.2 ⁹⁷
pentacene	0.76	1.83	1.95	2.04	2.05	2.05	2.1 ^{98,99}
quinacridone	1.43	2.76	3.02	3.13	3.13	3.11	
tetracene	1.26	2.46	2.72	2.78	2.80	2.79	3.3 ^{98,99}
anthracene	2.05	3.45	3.82	3.89	3.91	3.89	3.72 ¹⁰⁰
rubrene	1.15	2.32	2.70	2.77	2.79	2.77	2.67 ¹⁰¹
naphthalene	3.05	4.64	5.32	5.39	5.41	5.37	5.29 ^{98,99}
benzene	4.57	6.37	7.48	7.56	7.58	7.47	7.58 ^{98,99}
ammonia	4.52	6.82	8.76	9.00	9.17	8.92	
acetic acid	5.18	7.96	10.76	10.95	11.12	10.62	
H ₂ O (ice ^a)	5.42	7.92	10.96	11.23	11.49	10.94	10.9 ⁸³
ME (eV)	-2.05	-0.69	-0.12	-0.02	0.02	-0.06	–
MAE (eV)	2.05	0.70	0.19	0.18	0.21	0.16	–
MRE (%)	-49.6	-13.5	-4.9	-2.3	-1.7	-2.6	–
MARE (%)	49.6	13.8	6.1	5.1	5.4	4.9	–

^a See the Supplemental Material for details on the cell of ice used. The experimental photoemission gap shown is for proton-disordered ice Ih @ 80K.

static potential alignments computed at each level of theory). The results for PBE and PBE0 functionals did not provide very good agreement with experiment, whereas the sc-hybrid and RSH functional results appear to be in excellent agreement with experiment. However, we note that the experimental results in Table VI may not correspond to the cleaved surface used in our calculation, though the rubrene surface explored here is a typically exposed surface of that molecular crystal when deposited on an oxide surface (e.g. indium tin oxide or silica).¹⁰² In the case of ice, it appears that the sc-hybrid functional yields the best vertical ionization potential, but as shown by the gaps of Table V, not necessarily the best gap.

Finally we analyzed the photoelectron spectra of sev-

eral molecular crystals, including ice, rubrene, and pentacene. We found that the position of the highest excitation with respect to vacuum is accurately described by both RS DDH and DDH functionals. The comparison of the full spectra with the corresponding experimental results will be given elsewhere.

C. Finite Systems: Molecules and Nanoparticles

Here we investigate the applicability of the RSH functional form to finite systems, including molecules and nanoparticles. For finite systems $\epsilon_\infty \rightarrow 1$ and hence we discuss only the range-separated DDH. The generaliza-

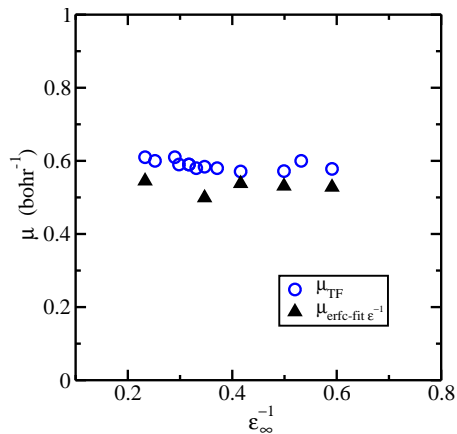


FIG. 5: (Color online) Several values of screening parameter μ (see text) plotted as a function of the inverse electronic dielectric constant (ϵ_{∞}^{-1}) for the set of molecular crystals of Table III. See Eq. (9) for μ_{TF} and Eq. (12) for $\mu_{\text{erfc-fit}}$.

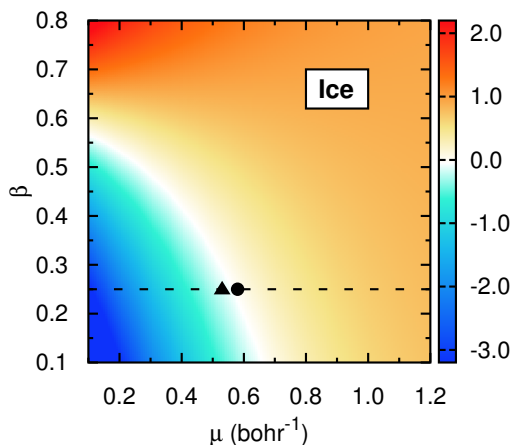


FIG. 6: (Color online) Signed electronic gap error of ice (theory - experiment), in units of eV, for a RSH functional defined by Eq. (7). Positive errors are indicated by shades of red colors and negative errors by shades of blue color. The white shaded area corresponds to zero error of the RSH with respect to experiment. The black dashed line is the short-range value of exact exchange for $\beta = 0.25$. The black circle and triangle indicate where the values of $\mu = \mu_{\text{TF}}$ and $\mu_{\text{erfc-fit}}$ fall, respectively.

tion of a full-range DDH functional to finite systems is presented in Ref. 107. In the case of molecules, we considered an additional screening parameter defined as:

$$\mu_{\alpha_M} = \left(\frac{1}{\alpha_M} \right)^{\frac{1}{3}} \quad (13)$$

where α_M is the molecular polarizability. We show below

TABLE VI: The vertical ionization potential (VIP_s), in units of eV, of several solid molecular crystals evaluated with PBE, PBE0, sc-hybrid and RSH functionals. The experimental values are listed for comparison. Note that for rubrene the surface listed corresponds to the orthorhombic cell. The screening parameters μ_{TF} and μ_{α_M} are defined in Eq. (9) and Eq. (13), respectively.

	surface	PBE	PBE0	schybrid	RSH	Exp.
		μ_{TF}				
rubrene	(100)	3.85	4.45	4.69	4.68	4.85 ¹⁰⁴
benzene	(001)	6.08	7.02	7.63	7.61	7.58 ⁹⁸
ice ^a	(10 $\bar{1}$ 0)	7.2	8.7	11.2	10.7	11.8 ^{105,106}

^a The prism surface of ice used. See Ref. 103 for further details on the common surfaces of ice.

TABLE VII: Screening parameters for isolated molecules. The second and third columns list the screening parameters obtained from the fit of the RPA dielectric function of the isolated molecules and obtained from the molecular polarizability radius (see Eq. (13)). We also give in column four the screening parameters obtained from the OT-RSH functional defined in Ref. 38.

	$\mu_{\text{erfc-fit}}$	μ_{α_M}	$\mu_{\text{OT-RSH}}$
C ₆₀ (buckminsterfullerene)	0.64	0.12	0.14
C ₂₄ H ₈ O ₆ (α PTCDA)	0.62	0.14	0.14
C ₂₂ H ₁₄ (pentacene)	0.56	0.14	0.15
C ₂₀ H ₁₂ O ₂ (β quinacridone)	0.59	0.15	0.15
C ₁₈ H ₁₂ (tetracene)	0.58	0.16	0.16
C ₁₄ H ₁₀ (anthracene)	0.59	0.18	0.18
C ₄₂ H ₂₈ (rubrene)	0.61	0.12	0.11
C ₁₀ H ₈ (naphthalene)	0.61	0.21	0.21
C ₆ H ₆ (benzene)	0.63	0.24	0.21
NH ₃ (ammonia)	0.63	0.40	0.33
C ₂ H ₄ O ₂ (acetic acid)	0.69	0.31	0.27
H ₂ O (water)	0.67	0.46	0.38

that a RSH form with $\mu = \mu_{\alpha_M}$ (Eq. (13)) yields results in good agreement with experiments; however if one chooses μ_{PDEP} (which yields accurate results for both inorganic and organic solids), the agreement with experiments for isolated molecules is worsened.

Table VII compares the screening parameters μ_{α_M} to $\mu_{\text{erfc-fit}}$ for molecules; we also compare to those obtained from the optimally tuned range-separated hybrid (OT-RSH)³⁸ procedure, where lr and sr fractions of exchange used in the OT-RSH to the same limits used in the present RS-DDH functional (i.e. lr = 1 and sr = 0.25). Interestingly, μ_{α_M} and $\mu_{\text{OT-RSH}}$ are very similar for several molecular systems and are loosely dependent on molecular size, whereas $\mu_{\text{erfc-fit}}$ is generally larger in value and nearly constant. Note that the advantage of using μ_{α_M}

TABLE VIII: The vertical ionization potentials (vIP) of the gas phase molecules that compose the molecular crystals are evaluated using the RS-DDH with $\mu = \mu_{\text{erfc-fit}}$, column 2, and $\mu = \mu_{\alpha_M}$, column 3, and with the OT-RSH functional defined in Ref. 38, column 4. The experimental values are listed for comparison in the last column. Unless otherwise noted they are taken from the NIST Webbook.¹⁰⁹

	vIP _g (eV)			
	RSH	RSH	RSH	Exp.
	$\mu_{\text{erfc-fit}}$	μ_{α_M}	$\mu_{\text{OT-RSH}}$	
C60	8.74	7.40	7.76	7.60
PTCDA	9.23	8.20	8.20	8.20
pentacene	7.08	6.29	6.29	6.61
quinacridone	8.44	7.35	7.35	7.23
tetracene	7.51	6.72	6.72	6.97
anthracene	8.14	7.30	7.30	7.44
rubrene	7.28	6.28	6.16	6.52
naphthalene	8.87	8.07	8.07	8.14
benzene	10.15	9.37	9.24	9.25
ammonia	11.85	11.07	10.7	10.8
acetic acid	12.61	11.08	10.78	10.9
H ₂ O	13.78	13.01	12.55	12.62
ME (eV)	0.95	-0.01	-0.10	-
MAE (eV)	0.95	0.19	0.14	-
MRE (%)	11.1	-0.6	-1.3	-
MARE (%)	11.1	2.3	1.9	-

over the optimization scheme of the OT-RSH functional lies in its ease of evaluation¹⁰⁸.

Table VIII lists the evaluated vertical ionization potentials using the RS-DDH functional with $\mu = \mu_{\text{erfc-fit}}$ and the molecular polarizability screening parameter (μ_{α_M}) for the gas phase molecules that compose the solid molecular crystals investigated in Section II B. The vertical ionization potentials using μ_{α_M} are in excellent agreement with experiment yielding a 2.3% MARE, whereas the electron affinities shown in Fig. S9 of the SM are described well for bound excited states (MARE of 9.9%). Using the screening parameter obtained from the complementary error function fit of the diagonal components of the dielectric matrix ($\mu_{\text{erfc-fit}}$) in the RS-DDH functional form to evaluate the vIP does not yield the same level of accuracy (MARE of 11.1%). Also shown in Table VIII are the vertical ionization potentials evaluated using the OT-RSH functional defined in Ref. 38, which are of the same level of accuracy as the RS-DDH with $\mu = \mu_{\alpha_M}$. The small difference seen in the MAEs for RS-DDH(μ_{α_M}) and OT-RSH is not statistically significant for the small set of molecules investigated (p-value of 0.18), indicating the two methods yield the same result.

We also computed the photoelectron spectra of several isolated molecules including benzene and pentacene, which are reported for various levels of theory in Fig. 7,

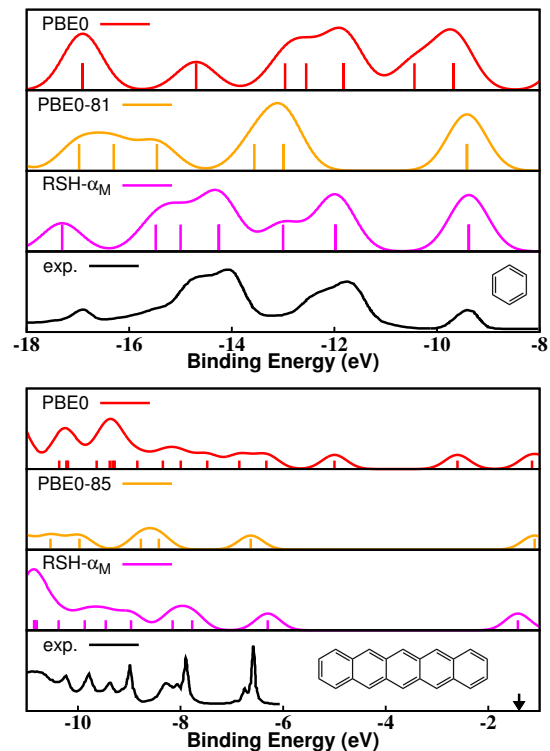


FIG. 7: (Color online) The photoelectron spectrum of isolated benzene (top panel) and pentacene (bottom panel) molecules at several levels of theory; PBE0 (red), PBE α^* ¹¹⁰ labeled as PBE0-81, and PBE0-85, in the top and bottom panels respectively (orange), RSH- α_M (magenta), and experiment (black). The computed spectra are broadened by a Gaussian of width 0.38 eV and 0.28 eV for benzene and pentacene, respectively. The black arrow indicates the experimental electron affinity for pentacene.

and compared to experiments. In the present work our focus is placed on the accurate determination of the spectra peak positions on an absolute scale rather than recovering the experimental peak intensities, and thus we did not formally compute intensities. The computed spectra shown are the density of states obtained by summing normalized gaussians centered at each KS energy state. For both molecules, the PBE0 spectra yield the poorest agreement with experiment. The highest occupied molecular orbital is best reproduced by the global hybrids PBE0-81 and PBE0-85, that minimize the difference between the KS eigenvalues and the GW quasi-particle corrections¹¹⁰:

$$\alpha^* = \arg \min_{\alpha} |\langle \psi_H(\alpha) | \Sigma(\alpha) - v_{xc}(\alpha) | \psi_H(\alpha) \rangle| \quad (14)$$

However these functionals yield a poor description of the rest of the spectra. A similar observation was previously pointed out by Körzdörfer *et al.*³⁹ in a study of tuned full-range hybrid functionals applied to molecules. Unlike full-range hybrid functionals, RSH introduces an

effective spatially dependent screening that treats differently each KS state according to their spatial extent. This offers additional flexibility and thus yields further improvement in the spectral features over the full-range hybrid functionals.

IV. SUMMARY AND CONCLUSIONS

In summary, we defined a range separated (RS) form of dielectric-dependent hybrid (DDH) functionals using material dependent, non empirical parameters and we showed that its performance is superior to that of non range-separated DDH functionals for the description of the electronic gap of a set of diverse inorganic semiconductors and insulators. The same functional form also yields results in excellent agreement with experiments for the electronic gaps and vertical ionization potentials of molecular crystals, with a performance similar to that of full-range DDHs. Finally we presented a generalization of RS-DDHs to molecules and we discussed which parameters are appropriate to bridge long and short range components of the generalized Kohn-Sham potential in the case of finite systems. The best agreement with experiments was obtained using a parameter related to the inverse of the cube root of the molecular polarizability, while the parameters used for extended systems (defined, e.g. using a Thomas-Fermi model fit to the diagonal components of the dielectric matrix) yielded less accurate results. We note in closing that the results presented here do not include the contribution from phonons coupling to

the electronic states, which may be significant for light element solids^{68–70,111}. Further analysis of the gap renormalization due to the electron-phonon coupling will be reported elsewhere.

ACKNOWLEDGMENTS

We thank Bartolomeo Civalleri and Roberto Orlando for useful discussions regarding the technical details of the methodological implementations in CRYSTAL14. We also would like to acknowledge both Ikutaro Hamada and Ding Pan for their insightful discussions. This work was supported by the NSF Center for Chemical Innovation—Powering the Planet, grant number NSF-CHE-0802907 (JHS) and by the Department of Energy grant DE-FG02-06ER46262 (MG and GG). An award of computer time was provided by the ASCR Leadership Computing Challenge (ALCC) program. This research used resources of the Argonne Leadership Computing Facility, which is a DOE Office of Science User Facility supported under Contract DE-AC02-06CH11357, resources of the National Energy Research Scientific Computing Center (NERSC), a DOE Office of Science User Facility supported by the Office of Science of the U.S. Department of Energy under Contract No. DE-AC02-05CH11231, resources of the Navy and Air Force DoD Supercomputing Resource Centers of the Department of Defense High Performance Computing Modernization Program, and resources of the University of Chicago Research Computing Center.

* Author to whom electronic correspondence should be addressed. Electronic address: gagalli@uchicago.edu

¹ R. Dreizler and E. Gross, *Density Functional Theory* (Springer Verlag, Berlin, 1990).

² V. Barone, *The Journal of chemical physics* **101**, 6834 (1994).

³ The basis representation common to the vast majority of quantum chemistry codes is instead localized basis sets (typically atom centered Gaussian functions).

⁴ X. Wu, A. Selloni, and R. Car, *Physical Review B* **79**, 085102 (2009).

⁵ F. Gygi, *Physical Review Letters* **102**, 166406 (2009).

⁶ M. Guidon, J. Hutter, and J. VandeVondele, *Journal of Chemical Theory and Computation* **6**, 2348 (2010).

⁷ F. Gygi and I. Duchemin, *Journal of Chemical Theory and Computation* **9**, 582 (2013).

⁸ T. Shimazaki and Y. Asai, *Chemical Physics Letters* **466**, 91 (2008).

⁹ T. Shimazaki and Y. Asai, *The Journal of chemical physics* **130**, 164702 (2009).

¹⁰ M. A. L. Marques, J. Vidal, M. J. T. Oliveira, L. Reining, and S. Botti, *Physical Review B* **83**, 035119 (2011).

¹¹ D. Koller, P. Blaha, and F. Tran, *Journal of Physics: Condensed Matter* **25**, 435503 (2013).

¹² J. H. Skone, M. Govoni, and G. Galli, *Physical Review B* **89** (2014), 10.1103/PhysRevB.89.195112.

¹³ S. Refaely-Abramson, S. Sharifzadeh, M. Jain, R. Baer, J. B. Neaton, and L. Kronik, *Physical Review B* **88**, 081204 (2013).

¹⁴ G. Pacchioni, *Catalysis Letters* (2014), 10.1007/s10562-014-1386-2.

¹⁵ M. Gerosa, C. E. Bottani, L. Caramella, G. Onida, C. Di Valentin, and G. Pacchioni, *Physical Review B* **91**, 155201 (2015).

¹⁶ M. Gerosa, C. Di Valentin, and C. E. Bottani, *The Journal of Chemical Physics* **143**, 111103 (2015).

¹⁷ M. Gerosa, C. E. Bottani, L. Caramella, G. Onida, C. Di Valentin, and G. Pacchioni, *The Journal of Chemical Physics* **143**, 134702 (2015).

¹⁸ J. M. Morbec, I. Narkeviciute, T. F. Jaramillo, and G. Galli, *Physical Review B* **90**, 155204 (2014).

¹⁹ J. M. Morbec and G. Galli, *Physical Review B* **93**, 035201 (2016).

²⁰ A. P. Gaiduk, M. Govoni, R. Seidel, J. H. Skone, B. Winter, and G. Galli, *Journal of the American Chemical Society* (accepted).

²¹ H. Seo, M. Govoni, and G. Galli, *Scientific Reports* **6**, 20803 (2016).

- ²² Z.-h. Yang, F. Sottile, and C. A. Ullrich, *Physical Review B* **92**, 035202 (2015).
- ²³ A. M. Ferrari, R. Orlando, and M. Rérat, *Journal of Chemical Theory and Computation* **11**, 3245 (2015).
- ²⁴ S. Refaely-Abramson, M. Jain, S. Sharifzadeh, J. B. Neaton, and L. Kronik, *Physical Review B* **92**, 081204 (2015).
- ²⁵ T. Shimazaki and T. Nakajima, *The Journal of chemical physics* **142**, 074109 (2015).
- ²⁶ J. Perdew, K. Burke, and M. Ernzerhof, *Physical Review Letters* **77**, 3865 (1996).
- ²⁷ P. Mori-Sánchez, A. J. Cohen, and W. Yang, *The Journal of chemical physics* **125**, 201102 (2006).
- ²⁸ J. Heyd, G. E. Scuseria, and M. Ernzerhof, *The Journal of chemical physics* **124**, 219906 (2006).
- ²⁹ D. Bylander and L. Kleinman, *Physical review. B, Condensed matter* **41**, 7868 (1990).
- ³⁰ With sX-LDA the local exchange and correlation potential used is LDA.
- ³¹ T. Yanai, D. P. Tew, and N. C. Handy, *Chemical Physics Letters* **393**, 51 (2004).
- ³² E. Weintraub and T. M. Henderson, *Journal of Chemical Theory and Computation* **5**, 754 (2009).
- ³³ J. E. Robinson, F. Bassani, R. S. Knox, and J. R. Schrieffer, *Phys. Rev. Letters* **9**, 215 (1962).
- ³⁴ S. J. Clark and J. Robertson, *Physical Review B* **82**, 085208 (2010).
- ³⁵ Y. Guo, J. Robertson, and S. J. Clark, *Journal of Physics: Condensed Matter* , 1 (2014).
- ³⁶ L. Hedin, *Physical Review* **139**, A796 (1965).
- ³⁷ R. Baer, E. Livshits, and U. Salzner, *Annual Review of Physical Chemistry* **61**, 85 (2010).
- ³⁸ S. Refaely-Abramson, S. Sharifzadeh, N. Govind, J. Autschbach, J. B. Neaton, R. Baer, and L. Kronik, *Physical Review Letters* **109**, 226405 (2012).
- ³⁹ T. Körzdörfer, R. M. Parrish, N. Marom, J. S. Sears, C. D. Sherrill, and J.-L. Brédas, *Physical Review B* **86**, 205110 (2012).
- ⁴⁰ I. Dabo, A. Ferretti, N. Poilvert, Y. Li, N. Marzari, and M. Cococcioni, *Physical Review B* **82**, 115121 (2010).
- ⁴¹ N. Poilvert, G. Borghi, N. L. Nguyen, N. D. Keilbart, K. Wang, and I. Dabo, *Koopmans-Compliant Self-Interaction Corrections*, 1st ed., Vol. 64 (Elsevier Inc., 2015).
- ⁴² N. L. Nguyen, G. Borghi, A. Ferretti, I. Dabo, and N. Marzari, *Physical Review Letters* **114**, 166405 (2015).
- ⁴³ $a_0 = (\frac{\hbar^2}{me^2})$.
- ⁴⁴ H. Wilson, F. Gygi, and G. Galli, *Physical Review B* **78**, 113303 (2008).
- ⁴⁵ M. Govoni and G. Galli, *Journal of Chemical Theory and Computation* **11**, 2680 (2015).
- ⁴⁶ PDEP here refers to the projective dielectric eigendecomposition technique used to evaluate the dielectric screening.
- ⁴⁷ M. Rérat, R. Orlando, and R. Dovesi, *Journal of Physics: Conference Series* **117**, 012016 (2008).
- ⁴⁸ B. G. Johnson and M. J. Frisch, *Chemical Physics Letters* **216**, 133 (1993).
- ⁴⁹ J. A. Pople, R. Krishnan, H. B. Schlegel, and J. S. Binkley, *International Journal of Quantum Chemistry* **16**, 225 (1979).
- ⁵⁰ G. J. B. Hurst, M. Dupuis, and E. Clementi, *The Journal of chemical physics* **89**, 385 (1988).
- ⁵¹ R. Orlando, M. Ferrero, M. Rérat, B. Kirtman, and R. Dovesi, *The Journal of chemical physics* **131**, 184105 (2009).
- ⁵² R. Dovesi, R. Orlando, A. Erba, C. M. Zicovich-Wilson, B. Civalleri, S. Casassa, L. Maschio, M. Ferrabone, M. De La Pierre, P. D'Arco, Y. Noël, M. Causà, M. Rérat, and B. Kirtman, *International Journal of Quantum Chemistry* **114**, 1287 (2014).
- ⁵³ P. Giannozzi, S. Baroni, N. Bonini, M. Calandra, R. Car, C. Cavazzoni, D. Ceresoli, G. L. Chiarotti, M. Cococcioni, I. Dabo, A. Dal Corso, S. de Gironcoli, S. Fabris, G. Fratesi, R. Gebauer, U. Gerstmann, C. Gougousis, A. Kokalj, M. Lazzeri, L. Martin-Samos, N. Marzari, F. Mauri, R. Mazzarello, S. Paolini, A. Pasquarello, L. Paulatto, C. Sbraccia, S. Scandolo, G. Sclauzero, A. P. Seitsonen, A. Smogunov, P. Umari, and R. M. Wentzcovitch, *Journal of Physics: Condensed Matter* **21**, 395502 (2009).
- ⁵⁴ F. Weigend and R. Ahlrichs, *Physical Chemistry Chemical Physics* **7**, 3297 (2005).
- ⁵⁵ D. Rappoport and F. Furche, *The Journal of Chemical Physics* **133**, 134105 (2010).
- ⁵⁶ M. F. Peintinger, D. V. Oliveira, and T. Bredow, *Journal of computational chemistry* **34**, 451 (2012).
- ⁵⁷ N. Troullier and J. Martins, *Physical review. B, Condensed matter* **43**, 1993 (1991).
- ⁵⁸ G. Makov and M. Payne, *Physical review. B, Condensed matter* **51**, 4014 (1995).
- ⁵⁹ For the present analysis, Ge was removed from the original test set because of uncertainties in the accuracy of the localized basis sets and pseudopotentials.
- ⁶⁰ Though the occupied valence bands of NiO and MnO have partial d-character, they also show a stronger hybridization with the oxygen 2p orbitals than the valence bands of CoO and FeO, and hence they are less localized. See Supplemental Material for further discussion.
- ⁶¹ M. Shishkin, M. Marsman, and G. Kresse, *Physical Review Letters* **99**, 246403 (2007).
- ⁶² C. Kittel, *Introduction to solid state physics* (Wiley, New York, 2005).
- ⁶³ B. Monemar, *Physical Review B* **8**, 5711 (1973).
- ⁶⁴ W. Choyke, D. Hamilton, and L. Patrick, *Physical Review* **133**, A1163 (1964).
- ⁶⁵ Y. Tezuka, S. Shin, T. Ishii, T. Ejima, S. Suzuki, and S. Sato, *Journal of the Physics Society Japan* **63**, 347 (1994).
- ⁶⁶ G. Sawatzky and J. Allen, *Physical Review Letters* **53**, 2339 (1984).
- ⁶⁷ C. D. Clark, P. J. Dean, and P. V. Harris, *Proceedings of the Royal Society A: Mathematical, Physical and Engineering Sciences* **277**, 312 (1964).
- ⁶⁸ M. Cardona, *Solid state communications* **133**, 3 (2005).
- ⁶⁹ F. Giustino, S. G. Louie, and M. L. Cohen, *Physical Review Letters* **105**, 265501 (2010).
- ⁷⁰ G. Antonius, S. Poncé, P. Boulanger, M. Côté, and X. Gonze, *Physical Review Letters* **112**, 215501 (2014).
- ⁷¹ J. van Elp, J. L. Wieland, H. Eskes, P. Kuiper, G. A. Sawatzky, F. M. F. de Groot, and T. S. Turner, *Phys. Rev. B* **44**, 6090 (1991).
- ⁷² G. Ramírez-Flores, H. Navarro-Contreras, A. Lastras-Martínez, R. C. Powell, and J. E. Greene, *Phys. Rev. B* **50**, 8433 (1994).
- ⁷³ J. Meyer, M. Kröger, S. Hamwi, F. Gnam, T. Riedl, W. Kowalsky, and A. Kahn, *Applied Physics Letters* **96**,

- 193302 (2010).
- ⁷⁴ M. Levinshtein, S. L. Rumyantsev, and M. S. Shur, *Properties of Advanced Semiconductor Materials: GaN, AlN, InN, BN, SiC, and SiGe* (Wiley, New York, 2001).
- ⁷⁵ S. Sayan, T. Emge, E. Garfunkel, X. Zhao, L. Wielunski, R. A. Bartynski, D. Vanderbilt, J. S. Suehle, S. Suzer, and M. Banaszak-Holl, *Journal of Applied Physics* **96**, 7485 (2004).
- ⁷⁶ L. Roskocová and J. Pastrňák, *Czechoslovak Journal of Physics B* **30**, 586 (1980).
- ⁷⁷ Ü. Özgür, Y. I. Alivov, C. Liu, A. Teke, M. A. Reshchikov, S. Doğan, V. Avrutin, S. J. Cho, and H. Morkoç, *Journal of Applied Physics* **98**, (2005).
- ⁷⁸ M. E. Innocenzi, R. T. Swimm, M. Bass, R. H. French, A. B. Villaverde, and M. R. Kokta, *Journal of Applied Physics* **67**, 7542 (1990).
- ⁷⁹ R. Whited, C. J. Flaten, and W. Walker, *Solid State Communications* **13**, 1903 (1973).
- ⁸⁰ G. Baldini and B. Bosacchi, *physica status solidi (b)* **38**, 325 (1970).
- ⁸¹ S.-i. Nakai and T. Sagawa, *Journal of the Physical Society of Japan* **26**, 1427 (1969).
- ⁸² M. Piacentini, D. W. Lynch, and C. G. Olson, *Phys. Rev. B* **13**, 5530 (1976).
- ⁸³ K. Kobayashi, *The Journal of Physical Chemistry* **87**, 4317 (1983).
- ⁸⁴ N. Schwentner, F. J. Himpsel, V. Saile, M. Skibowski, W. Steinmann, and E. E. Koch, *Phys. Rev. Lett.* **34**, 528 (1975).
- ⁸⁵ F. Wilcoxon, *Biometrics Bulletin* **1**, 80 (1945).
- ⁸⁶ D. F. Bauer, *Journal of the American Statistical Association* **67**, 687 (1972).
- ⁸⁷ P. G. Cummins and D. A. Dunmur, *Journal of Physics D: Applied Physics* (1974).
- ⁸⁸ M. I. Alonso, M. Garriga, N. Karl, J. O. Ossó, and F. Schreiber, *Organic Electronics* (2002).
- ⁸⁹ R. W. Munn, *The Journal of chemical physics* **58**, 3828 (1973).
- ⁹⁰ D. Y. Zang, F. F. So, and S. R. Forrest, *Applied Physics Letters* **59**, 823 (1991).
- ⁹¹ N. Karl, H. Rohrbacher, and D. Siebert, *physica status solidi (a)* **4**, 105 (1971).
- ⁹² H. Fuchigami, S. Tanimura, Y. Uehara, T. Kurata, and S. Tsunoda, *Japanese Journal of Applied Physics* **34**, 3852 (1995).
- ⁹³ In the present RS DDH the dielectric constant and consequently the fraction of exchange is an average over all directions. Computing quantities such as charge transfer integrals¹¹² would likely require a more explicit handling of the directional screening, e.g. by evaluating the full dielectric screening matrix W in GW based methods.
- ⁹⁴ A. Fonari, C. Sutton, J.-L. Brédas, and V. Coropceanu, *Physical Review B* **90**, 165205 (2014).
- ⁹⁵ C. A. Guido, E. Brémont, C. Adamo, and P. Cortona, *The Journal of chemical physics* **138**, 021104 (2013).
- ⁹⁶ R. W. Lof, M. A. Van Veenendaal, and B. Koopmans, *Physical Review* (1992).
- ⁹⁷ D. R. T. Zahn, G. N. Gavrila, and M. Gorgoi, *Chemical Physics* **325**, 99 (2006).
- ⁹⁸ N. Sato, K. Seki, and H. Inokuchi, *Journal of the Chemical Society, Faraday Transactions 2* **77**, 1621 (1981).
- ⁹⁹ C. D. Lindstrom, M. Muntwiler, and X.-Y. Zhu, *The journal of physical chemistry. B* **111**, 6913 (2007).
- ¹⁰⁰ G. Vaubel and H. Baessler, *Physics Letters A* (1968).
- ¹⁰¹ H. Ding and Y. Gao, *Applied Physics A* **95**, 89 (2009).
- ¹⁰² X.-K. Chen, Y.-T. Fu, H. Li, and J.-L. Brédas, *Advanced Materials Interfaces* **1**, 1400362 (2014).
- ¹⁰³ D. Pan, L.-M. Liu, G. A. Tribello, B. Slater, A. Michaelides, and E. Wang, *Journal of Physics: Condensed Matter* **22**, 074209 (2010).
- ¹⁰⁴ Y. Nakayama, S. Machida, T. Minari, K. Tsukagoshi, Y. Noguchi, and H. Ishii, *Applied Physics Letters* **93**, 173305 (2008).
- ¹⁰⁵ B. Winter, R. Weber, W. Widdra, M. Dittmar, M. Faubel, and I. V. Hertel, *The Journal of Physical Chemistry A* **108**, 2625 (2004).
- ¹⁰⁶ D. Nordlund, H. Ogasawara, and A. Nilsson, *Maxlab Annual Report*, 236 (2001).
- ¹⁰⁷ N. Brawand, M. Voros, M. Govoni, and G. Galli, Submitted (2016).
- ¹⁰⁸ The difference between the RS-DDH and the OT-RSH resides in the evaluation of the screening parameter; the former determined from linear response theory and the latter from an ionization potential tuning procedure.
- ¹⁰⁹ P. Linstrom and W. Mallard, *NIST Chemistry WebBook, NIST Standard Reference Database Number 69* (National Institute of Standards and Technology, Gaithersburg MD, 2001).
- ¹¹⁰ V. Atalla, M. Yoon, F. Caruso, P. Rinke, and M. Scheffler, *Physical Review B* **88**, 165122 (2013).
- ¹¹¹ B. Monserrat, E. A. Engel, and R. J. Needs, *Phys. Rev. B* **92**, 140302 (2015).
- ¹¹² A. Fonari, N. S. Corbin, D. Vermeulen, K. P. Goetz, O. D. Jurchescu, L. E. McNeil, J. L. Bredas, and V. Coropceanu, *The Journal of Chemical Physics* **143**, 224503 (2015).